

Reproduction of Experimental Gap Structure in LiFeAs based on the Orbital-Spin Fluctuation Theory: s_{++} -wave, s_{\pm} -wave, and hole- s_{\pm} -wave states

Tetsuro SAITO¹, Seiichiro ONARI², Youichi YAMAKAWA¹, Hiroshi KONTANI¹, Sergey V. Borisenko³, and Volodymyr B. Zabolotny³

¹ *Department of Physics, Nagoya University, Furo-cho, Nagoya 464-8602, Japan.*

² *Department of Applied Physics, Nagoya University, Furo-cho, Nagoya 464-8603, Japan.*

³ *Leibniz-Institute for Solid State Research, IFW-Dresden, D-01171 Dresden, Germany*

(Dated: September 25, 2018)

The absence of nesting between electron and hole-pockets in LiFeAs with $T_c = 18\text{K}$ attracts great attention, as an important hint to understand the pairing mechanism of Fe-based superconductors. Here, we study the five-orbital model of LiFeAs based on the recently-developed orbital-spin fluctuation theories. It is found that the experimentally observed gap structure of LiFeAs, which is a “fingerprint” of the pairing mechanism, is quantitatively reproduced in terms of the orbital-fluctuation-mediated s_{++} -wave state. Especially, the largest gap observed on the small two hole-pockets composed of (d_{xz}, d_{yz}) orbitals can be explained, and this is a hallmark of the orbital-fluctuation-mediated superconductivity. The s_{++} -wave gap structure becomes more anisotropic in the presence of weak spin fluctuations. As the spin fluctuations increase, we obtain the “hole- s_{\pm} -wave state”, in which only the gap of the large hole-pocket made of d_{xy} -orbital is sign-reversed, due to the cooperation of orbital and spin fluctuations. This gap structure with “sign-reversal between hole-pockets” is similar to that recently reported in $(\text{Ba,K})\text{Fe}_2\text{As}_2$.

PACS numbers: 74.70.Xa, 74.20.-z, 74.20.Rp

I. INTRODUCTION

The most remarkable feature of Fe-based superconductors would be the amazing variety of the normal and superconducting states in various materials. The high- T_c state with $T_c > 30\text{K}$ is realized by electron-doping, hole-doping, in addition to isovalent-doping, irrespective of the huge change of the Fermi surfaces (FSs). In Ba122 systems, the superconducting phase is next to the orthorhombic (C_2) structure phase, accompanied by the magnetic order. Near the structural and magnetic quantum critical points, strong orbital and spin fluctuations are observed [1–7], and these fluctuations would be the origin of superconductivity. In $\text{FeSe}_x\text{Te}_{1-x}$, in contrast, the optimum T_c is realized near the structural quantum-critical-point at $x \approx 0.6$ [8], whereas magnetic order is absent for $x > 0.4$. In heavily H-doped La1111 and (La,P) co-doped Ca122, high- T_c above 40K is realized near the isostructural (C_4) transition phase.

Also, the shape of the FSs, which is essential for the electronic properties of each material, is strongly material-dependent [9]: In La1111, the band structure is almost two-dimensional and the FSs are mainly composed of the d_{xz} , d_{yz} and d_{xy} orbitals. In Ba122, the band structure has three-dimensional character, and the $d_{3z^2-r^2}$ orbital also contributes to the FS. In $\text{FeSe}_x\text{Te}_{1-x}$, the Fermi momentum k_F is less than one-fifth of that of Ba122, and the Fermi energy is just $\sim 100\text{K}$ [10]. In heavily H-doped La1111 and (La,P) co-doped Ca122, high- T_c ($\gtrsim 40\text{K}$) is realized irrespective that the hole-pockets are very tiny or absent. These experimental facts strongly indicate the wide variety of the pairing mechanisms in Fe-based superconductors, and quantitative analysis based on the realistic tight-binding model is required for each

compound.

Up to now, the spin-fluctuation-mediated s_{\pm} -wave state with sign-reversal between hole- and electron-pockets had been studied by many authors [11–14]. In La1111 systems, however, the relation between the strength of spin fluctuations and T_c is less clear. For example, T_c of 14% F-doped LaFeAsO increases from 23K to 43K by applying the pressure 3GPa, although the $1/T_1$ remains small and almost unchanged. Later, the orbital-fluctuation-mediated s_{++} -wave state without sign-reversal had been proposed [15, 16]. The robustness of T_c against the randomness in various Fe-pnictides [17–19] is consistent with the s_{++} -wave state [20, 21]. Also, resonance-like peak in the neutron scattering spectrum is explained in term of the s_{++} -wave state by taking the realistic inelastic scattering into account [22].

In the study of the pairing mechanism, the detailed gap structure given by the angle-resolved-photoemission-spectroscopy (ARPES) offers us very useful information. For this purpose, LiFeAs ($T_c = 18\text{K}$) is favorable since very clean single crystals can be synthesized. For this reason, the intrinsic gap structure free from the impurity effect can be obtained in the case of LiFeAs. The detailed gap structure of LiFeAs had been obtained by ARPES [23, 24]. The FSs given in Ref. [23] are shown in Fig. 1 (a), which are reproduced by the ten-orbital tight-binding model (two-Fe unit cell). Figure 1 (b) shows the FSs in the five-orbital model (single Fe unit cell) obtained by unfolding the original ten-orbital model. Both models are equivalent mathematically, and the unfolding is performed by following the procedure in Ref. [25].

The bad nesting in LiFeAs between hole-like FSs (h-FSs) and electron-like FSs (e-FSs) attracts great attention, as an important hint to understand the variety and

commonness of the pairing mechanism in Fe-based superconductors. Consistently, the observed spin fluctuations are moderate according to NMR measurements [26] and neutron scattering measurements [27–29].

In Ref. [30], the spin fluctuation mediated s_{\pm} -wave state had been studied based on the ten-orbital model for LiFeAs. The obtained gap functions on the tiny hole-pockets h-FS1 and h-FS2 in Fig. 1 (b) are very small when the filling of electrons per Fe-site is $n = 6.0$, although they are the largest in the ARPES measurement [23, 24] and the Scanning Tunneling Microscopy (STM) measurement [31]. Thus, it is an important challenge to verify to what extent the experimental gap structure is reproduced based on the orbital fluctuation theories.

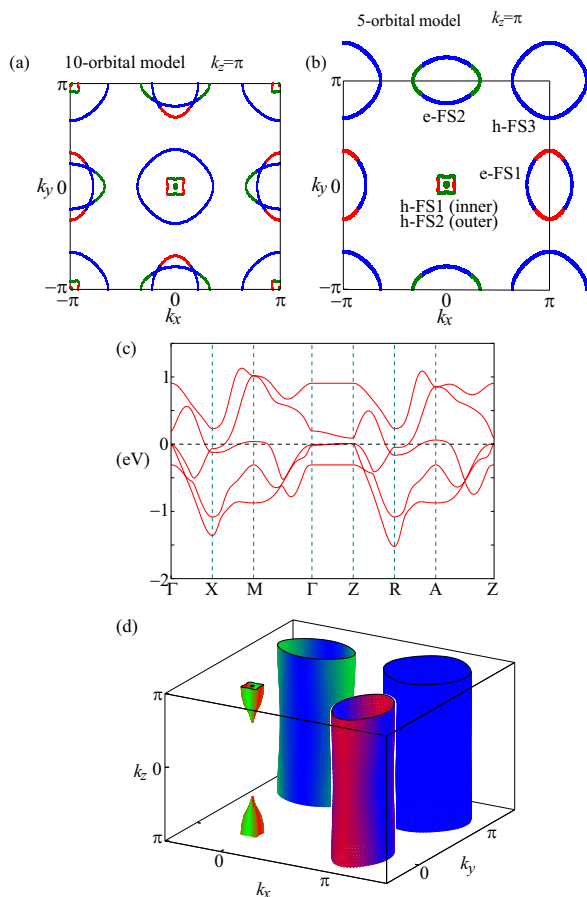


FIG. 1: (Color online) The FSs in the $k_z = \pi$ plane of the three-dimensional ten-orbital model (a) and five-orbital model (b) for LiFeAs. The green, red and blue lines correspond to xz , yz and xy orbitals, respectively. In (b), h-FS1,2,3 are hole-like, and e-FS1,2 are electron-like. (c) The dispersion of the band structure of the five-orbital model. (d) The three-dimensional shape of the FSs of the five-orbital model.

In this paper, we study the five-orbital model of LiFeAs based on the recently-developed orbital-spin fluctuation theories [15, 16]. When only the orbital fluctuations develop, the anisotropic s_{++} -wave state without sign-reversal is obtained. In this case, experimentally ob-

served gap structure of LiFeAs, especially the largest gap experimentally observed on h-FS1 and h-FS2, is quantitatively reproduced. This is a hallmark of the orbital-fluctuation-mediated superconductivity since the spin fluctuation scenario predicts the smallest gap on h-FS1 and h-FS2. When orbital and spin fluctuations coexist, we can obtain the “hole- s_{\pm} -wave state”, in which the gap structure with “sign-reversal between hole-pockets” is realized. This exotic gap structure had been discussed in $(\text{Ba,K})\text{Fe}_2\text{As}_2$ experimentally, [32, 33] and it might be realized in other Fe-based superconductors.

We stress that the experimental gap structure is a “fingerprint” of the pairing mechanism. For example, in Ba122 and Sr122, the “horizontal-node” on the $d_{3z^2-r^2}$ -orbital h-FS around the Z point was predicted by spin fluctuation theories [34, 35], since $d_{3z^2-r^2}$ -orbital is absent on the e-FSs. In contrast, the horizontal-node is absent in the orbital-fluctuation-mediated s -wave state, due to the strong inter-orbital fluctuations [35]. The latter is supported by recent ARPES measurements for optimal $\text{BaFe}_2(\text{As,P})_2$ [36, 37] and in-plane field angle dependence of the thermal conductivity [38].

II. FORMALISM

In this paper, we set x and y axes parallel to the nearest Fe-Fe bonds, and the orbital z^2 , xz , yz , xy , and $x^2 - y^2$ are denoted as 1, 2, 3, 4, and 5 respectively. The three-dimensional ten-orbital tight-binding model had been obtained in Ref. [30] by fitting the experimentally observed dispersion reported in Ref. [23], and its FSs are shown in Fig. 1 (a). In this model, the band renormalization due to the mass enhancement $m^*/m_b \sim 2$ is taken into account. To simplify the numerical calculation, we derive the five-orbital model by unfolding the original ten-orbital model [25]. The FSs and the band dispersion of the five-orbital model are shown in Fig. 1 (b) and (c), respectively. The three-dimensional FSs of the five-orbital model are shown in Fig. 1 (d).

The kinetic term of the five-orbital model is given as

$$\begin{aligned} \hat{H}^0 &= \sum_{ablm\sigma} t_{l,m}(\mathbf{R}_a - \mathbf{R}_b) c_{l\sigma}^\dagger(\mathbf{R}_a) c_{m\sigma}(\mathbf{R}_b) \\ &= \sum_{klm\sigma} \left\{ \sum_a t_{l,m}(\mathbf{R}_a) e^{i\mathbf{k} \cdot \mathbf{R}_a} \right\} c_{l\sigma}^\dagger(\mathbf{k}) c_{m\sigma}(\mathbf{k}), \quad (1) \end{aligned}$$

where a, b represent the Fe-sites, $l, m = 1 - 5$ represent the d orbital, and $\sigma = \pm 1$ is the spin index. \mathbf{R}_a is the position of Fe-site, $c_{l\sigma}^\dagger(\mathbf{R}_a)$ is the creation operator of the d electron, and $t^{l,m}(\mathbf{R}_a)$ is the hopping integral. The values of $t_{a,b}^{l,m}$ are shown in Appendix B. Figure 2 (a) and (b) show the inverse of the Fermi velocity on the i -th FS, $1/v_F^i(\mathbf{k})$, in $k_z = 0$ and $k_z = \pi$ planes, respectively. The horizontal axis is $\theta = \tan^{-1}(\bar{k}_y/\bar{k}_x)$, where (\bar{k}_x, \bar{k}_y) is the momentum on the FS with the origin at the center of each pocket. Figure 2 (c)-(f) show the l -orbital weight

on the i -th FS, given by $|U_{l,i}(\mathbf{k})|^2 = |\langle \mathbf{k}, l | \mathbf{k}, i \rangle|^2$ at the Fermi momentum.

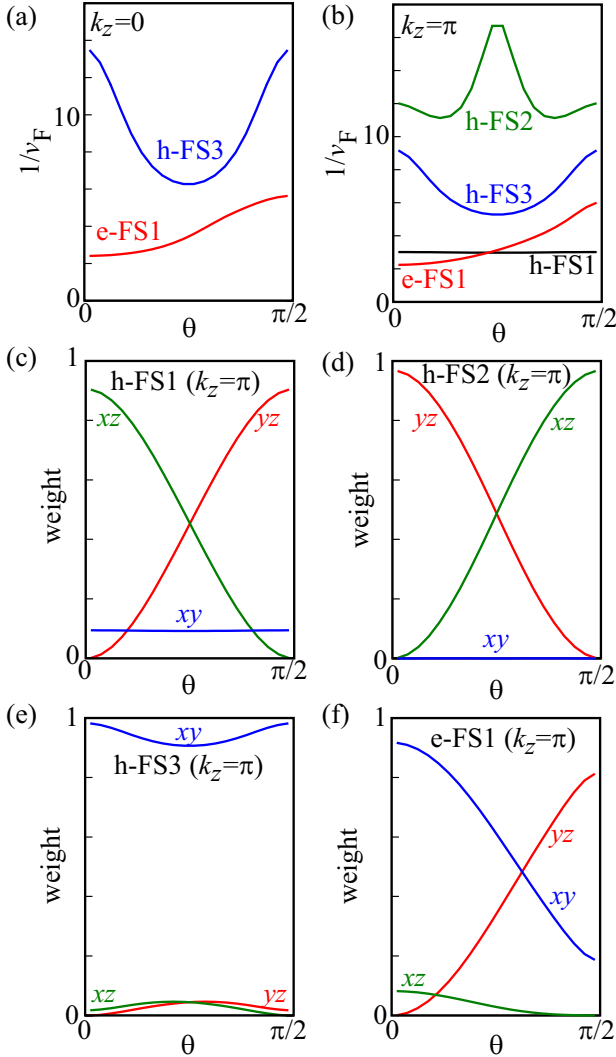


FIG. 2: (Color online) (a,b) Inverse of the Fermi velocity on the i -th FS $1/v_F^i(\mathbf{k})$. The horizontal axis is $\theta = \tan^{-1}(k_y/k_x)$. (c-f) The weight of each d -orbital on the i -th FS.

Next, we explain the interaction term. We introduce both the Coulomb interaction (U , U' , $J = (U - U')/2$) and quadrupole interaction. The latter are induced by the electron-phonon (e-ph) interaction due to Fe ion oscillations as follows, [15]

$$V_{\text{quad}} = -g(\omega_l) \sum_a^{\text{site}} \left(\hat{O}_{yz}^a \cdot \hat{O}_{yz}^a + \hat{O}_{xz}^a \cdot \hat{O}_{xz}^a \right), \quad (2)$$

where $g(\omega_l) = g \cdot \omega_0^2 / (\omega_l^2 + \omega_0^2)$, and $g = g(0)$ is the quadrupole interaction at $\omega_l = 0$. ω_0 is the cutoff energy of the quadrupole interaction. $\hat{O}_\Gamma^a = \sum_{l,m} o_\Gamma^{l,m} \hat{m}_{l,m}^a$ ($\hat{m}_{l,m}^a = \sum_\sigma c_{l\sigma}^\dagger(\mathbf{R}_a) c_{m\sigma}(\mathbf{R}_a)$) is the quadrupole operator at site \mathbf{R}_a introduced in Ref. [15]: The non-zero coefficients of $o_\Gamma^{l,m} = o_\Gamma^{m,l}$ are $o_{xz}^{2,5} = o_{xz}^{3,4} = \sqrt{3}o_{xz}^{1,2} = 1$, and

$-o_{yz}^{3,5} = o_{yz}^{2,4} = \sqrt{3}o_{yz}^{1,3} = 1$. Thus, \hat{V}_{quad} has many non-zero inter-orbital elements. As explained in Ref. [15], g is induced by in-plane Fe-ion oscillations. Also, the Aslamazov-Larkin type vertex correction (AL-VC) due to Coulomb interaction produces large effective quadrupole interaction g [16]. Thus, the quadrupole interaction in eq. (2) is derived from both mechanisms.

Now, we perform the RPA for the present model, by using $64 \times 64 \times 16$ \mathbf{k} meshes. We fix the temperature at $T = 0.01$ eV, and set the filling of each Fe-site as $n = 6.0$. Hereafter, the unit of energy as eV. The irreducible susceptibility in the five-orbital model is given by

$$\chi_{ll',mm'}^{(0)}(q) = -\frac{T}{N} \sum_k G_{l,m}^{(0)}(k+q) G_{m',l'}^{(0)}(k), \quad (3)$$

where $q = (\mathbf{q}, \omega_l)$ and $k = (\mathbf{k}, \epsilon_n)$. $\epsilon_n = (2n+1)\pi T$ and $\omega_l = 2l\pi T$ are the fermion and boson Matsubara frequencies. $\hat{G}^{(0)}(k) = [i\epsilon_n + \mu - \hat{h}_k^{(0)}]^{-1}$ is the Green function in the orbital basis, where $\hat{h}_k^{(0)}$ is the matrix representation of $\hat{H}^{(0)}$ and μ is the chemical potential. In the RPA, the susceptibilities for spin and charge sectors are given by [39]

$$\hat{\chi}^s(q) = \frac{\hat{\chi}^{(0)}(q)}{\hat{1} - \hat{\Gamma}^s \hat{\chi}^{(0)}(q)}, \quad (4)$$

$$\hat{\chi}^c(q) = \frac{\hat{\chi}^{(0)}(q)}{\hat{1} - \hat{\Gamma}_g^c(\omega_l) \hat{\chi}^{(0)}(q)}, \quad (5)$$

where

$$(\hat{\Gamma}^s)_{l_1 l_2, l_3 l_4} = \begin{cases} U, & l_1 = l_2 = l_3 = l_4 \\ U', & l_1 = l_3 \neq l_2 = l_4 \\ J, & l_1 = l_2 \neq l_3 = l_4 \\ J', & l_1 = l_4 \neq l_2 = l_3 \\ 0, & \text{otherwise} \end{cases} \quad (6)$$

$$\hat{\Gamma}_g^c(\omega_l) = \hat{\Gamma}^c - 2\hat{V}_{\text{quad}}(\omega_l), \quad (7)$$

$$(\hat{\Gamma}^c)_{l_1 l_2, l_3 l_4} = \begin{cases} -U, & l_1 = l_2 = l_3 = l_4 \\ U' - 2J, & l_1 = l_3 \neq l_2 = l_4 \\ -2U' + J, & l_1 = l_2 \neq l_3 = l_4 \\ -J', & l_1 = l_4 \neq l_2 = l_3 \\ 0, & \text{otherwise} \end{cases} \quad (8)$$

In the RPA, the enhancement of the spin susceptibility $\hat{\chi}^s$ is mainly caused by the intra-orbital Coulomb interaction U , using the ‘‘intra-orbital nesting’’ of the FSs. On the other hand, the enhancement of $\hat{\chi}^c$ in the present model is caused by the quadrupole-quadrupole interaction in eq. (2), utilizing the ‘‘inter-orbital nesting’’ of the FSs. The magnetic (orbital) order is realized when the spin (charge) Stoner factor α_s (α_c), which is the maximum eigenvalue of $\hat{\Gamma}^s \hat{\chi}^{(0)}(\mathbf{q}, 0)$, ($\hat{\Gamma}_g^c(0) \hat{\chi}^{(0)}(\mathbf{q}, 0)$), is

unity. Here, the critical value of U is $U_{\text{cr}} = 0.448$ eV, and the critical value of g is $g_{\text{cr}} = 0.132$ eV for $U = 0$. (We note again that the band renormalization due to the mass enhancement $m^*/m_b \sim 2$ is taken into account in the present tight-binding model.)

Figure 3 (a) shows the obtained spin susceptibility $\chi^s(\mathbf{q}, 0) \equiv \sum_{l,m} \chi_{l,l:m,m}^s(\mathbf{q}, 0)$ in the $q_z = 0$ plane given by the RPA for $U = 0.439$ and $g = 0$. The spin Stoner factor is $\alpha_s = 0.98$. At $T = 0.01$, the obtained peak is incommensurate at (π, δ) with $\delta \approx 0.1\pi$, consistently with the recent neutron scattering experiment [28]. The relation $\chi_{4,4;4,4}^s(\mathbf{q}, 0) \gg \chi_{2,2;2,2}^s(\mathbf{q}, 0), \chi_{3,3;3,3}^s(\mathbf{q}, 0)$ holds in the present model, due to the intra d_{xy} -orbital nesting between h-FS3 and e-FS. That is, the spin fluctuations develop mainly on the d_{xy} -orbital.

Figure 3 (b) shows the quadrupole susceptibility $\chi_{\Gamma}^Q(\mathbf{q}, 0) = \sum_{l,l',m,m'} o_{\Gamma}^{l,l'} \chi_{l,l':m,m'}^c(\mathbf{q}, 0) o_{\Gamma}^{m',m}$ for the channel $\Gamma = xz$ in the $q_z = 0$ plane. The charge Stoner factor is $\alpha_c = 0.98$. In this model, both $\chi_{xz}^Q(\mathbf{q}, 0)$ and $\chi_{yz}^Q(\mathbf{q}, 0)$ are the most divergent channels. For $\Gamma = xz$, the dominant contribution comes from $\chi_{3,4;4,3}^c(\mathbf{q}, 0) \approx \chi_{3,4;3,4}^c(\mathbf{q}, 0)$, due to the inter-orbital nesting (orbital 3 and 4) between h-FS1,2 and e-FS1. The obtained $\chi_{xz}^Q(\mathbf{q}, 0)$ shows broad peak around (π, δ) with $|\delta| \lesssim 0.2\pi$.

We note that both $\chi_{xz}^Q(\mathbf{q}, 0)$ and $\chi^s(\mathbf{q}, 0)$ are almost independent of q_z . That is, both the orbital and spin fluctuations are almost two-dimensional.

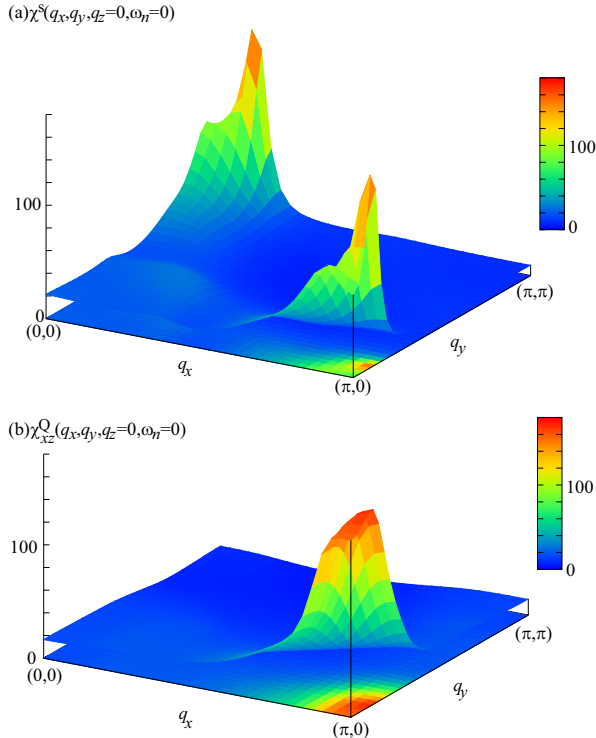


FIG. 3: (Color online) (a) Obtained spin susceptibility $\chi^s(\mathbf{q}, 0)$ for $U = 0.98U_{\text{cr}}$ and $g = 0$. The spin fluctuations develop mainly on the d_{xy} -orbital. (b) Obtained O_{xz} -channel quadrupole susceptibility $\chi_{xz}^Q(\mathbf{q}, 0)$ for $U = 0$ and $g = 0.98g_{\text{cr}}$, developed among the d_{xz}/d_{yz} -orbitals.

Next, we solve the linearized Eliashberg equation based on the three-dimensional model of LiFeAs. In order to obtain the fine momentum dependence of the SC gap, we concentrate on the gap functions only on the FSs as done in Ref. [40]: We used 80×16 \mathbf{k} points for each Fermi surface sheet. Without impurities, the linearized Eliashberg equation is given as [40]

$$\lambda_E \Delta^i(\mathbf{k}, \epsilon_n) = \frac{\pi T}{(2\pi)^3} \sum_{\epsilon_m} \sum_j^{\text{FS}} \int_{\text{FS}_j} \frac{d\mathbf{k}'_{\text{FS}_j}}{v^j(\mathbf{k}')} \times V^{ij}(\mathbf{k}, \mathbf{k}', \epsilon_n - \epsilon_m) \frac{\Delta^j(\mathbf{k}', \epsilon_m)}{|\epsilon_m|}, \quad (9)$$

where λ_E is the eigenvalue that reaches unity at $T = T_c$. i and j denote the FSs, and $\Delta^i(\mathbf{k}, \epsilon_n)$ is the gap function on the i -th FS at the Fermi momentum \mathbf{k} . The integral in eq. (9) means the surface integral on the j -th FS. The pairing interaction V in eq. (9) is

$$V^{ij}(\mathbf{k}, \mathbf{k}', \epsilon_n - \epsilon_m) = \sum_{l_i} U_{l_i, i}^*(\mathbf{k}) U_{l_i, i}(\mathbf{k}) \times V_{l_1 l_2, l_3 l_4}(\mathbf{k} - \mathbf{k}', \epsilon_n - \epsilon_m) U_{l_2, j}(\mathbf{k}') U_{l_3, j}^*(\mathbf{k}'), \quad (10)$$

$$\hat{V} = \hat{V}^c + \hat{V}^s + \hat{V}^{(0)}, \quad (11)$$

$$\hat{V}^c = \frac{1}{2} \hat{\Gamma}_g^c \hat{\chi}^c \hat{\Gamma}_g^c, \quad \hat{V}^s = -\frac{3}{2} \hat{\Gamma}_s^s \hat{\chi}^s \hat{\Gamma}_s^s, \quad (12)$$

$$\hat{V}^{(0)} = \frac{1}{2} (\hat{\Gamma}_g^c - \hat{\Gamma}_s^s), \quad (13)$$

where $U_{l_i, i}(\mathbf{k}) = \langle \mathbf{k}; l | \mathbf{k}; i \rangle$ is the transformation unitary matrix between the band and the orbital representations.

In this calculation, we simplify the energy dependence of \hat{V} . We assume that \hat{V}^ξ ($\xi = c, s$) can be separated into the momentum and orbital dependent part $\hat{V}^\xi(\mathbf{k}, \omega_l = 0)$ and energy dependent part $g_\xi(\omega_l)$:

$$\hat{V}^\xi(\mathbf{k}, \omega_l) = \hat{V}^\xi(\mathbf{k}, \omega_l = 0) \times g_\xi(\omega_l). \quad (14)$$

We calculated $\hat{V}^\xi(\mathbf{k}, \omega_l = 0)$ without approximation. On the other hand, $g_\xi(\omega_l)$ is determined as

$$g_\xi(\omega_l) = \text{Re} \left[\frac{V_{\text{max}}^\xi(\omega_l)}{V_{\text{max}}^\xi(\omega_l = 0)} \right], \quad (15)$$

where $V_{\text{max}}^\xi(0)$ is the largest value of $V_{l_1 l_2, l_3 l_4}^\xi(\mathbf{k}, \omega_l = 0)$ for any $\{l_i\}$ and \mathbf{k} . It is verified that this simplification affects the momentum dependence of the SC gap functions only quantitatively, although the obtained λ_E is slightly underestimated. Thus, this approximation would be appropriate for the present purpose, that is, the analysis of the anisotropy of the SC gap.

III. SUPERCONDUCTING GAP FUNCTIONS

In this section, we analyze the linearized Eliashberg equation, eq.(9), and obtain the three-dimensional gap

function $\Delta^i(\theta, k_z)$, defined on the Fermi surface sheet i . Here, we divide the variables $\theta = [0, 2\pi]$ and $k_z = [-\pi, \pi]$ into 80 and 16 meshes, respectively, and use 512 Matsubara frequencies. The pairing interaction in eq. (10) is given by the RPA, assuming that $J = J'$ and $U = U' + 2J$, and fix the ratio $J/U = 1/6$. The used parameters are $T = 0.01$ and $\omega_0 = 0.02$.

A. Orbital-fluctuation-mediated S_{++} -wave state

We first discuss the s_{++} -wave state realized by orbital fluctuations: Figure 4 (a) shows the obtained gap functions in the case of $g = 0.129$ and $U = 0$ ($\alpha_c = 0.98$) in the $k_z = \pi$ -plane. As for the hole-pockets, the gap functions on the h-FS1,2 composed of (d_{xz}, d_{yz}) -orbitals are the largest, while the gap on the h-FS3 composed of d_{xy} -orbital is the smallest. These results are quantitatively consistent with the experimental data [23] shown in dotted lines. (We adjust the magnitude of gap functions since it cannot be determined by solving the linearized gap equation.)

As for the electron-pockets, the gap function has the local maxima at $\theta = 0$, and the minimum point is $\theta \approx 0.4\pi$. This result is also consistent with the experimental data [23]. In Appendix A, we show the s_{++} -wave gap for smaller g ($\alpha_c = 0.90$), and find that the gap structure is essentially independent of the strength of orbital fluctuations. Therefore, overall experimental data are quantitatively reproduced by the orbital fluctuation theory. In Fig. 4 (b), we show the three-dimensional gap structure. The gap function on each FS is almost independent of k_z . Note that h-FS1 and h-FS2 appear only for $k_z \approx \pm\pi$; see Fig. 1 (d).

In Fig. 4 (c), we discuss the origin of the orbital- and FS-dependences of the gap functions: The broad peak of the quadruple susceptibility $\chi_{xz}^Q(\mathbf{q}, 0)$ at $\mathbf{q} \approx (\pi, \delta)$ with $|\delta| \lesssim 0.2\pi$ in Fig. 3 (b) is mainly given by the inter-orbital nesting between h-FS1,2 (orbital 2,3) and e-FS1 (orbital 4). For this reason, the maximum gap is realized on h-FS1 (Δ_1^h), h-FS2 (Δ_2^h), and e-FS1 (Δ_1^e) at $\theta = 0$. The gap size of h-FS3 (Δ_3^h) is the smallest, and its maximum is located at $\theta = \pi/4$. Therefore, the experimentally observed gap functions are understood based on the orbital fluctuation theory very well.

B. Spin-fluctuation-mediated S_{\pm} -wave state

Next, we discuss the s_{\pm} -wave state realized by spin fluctuations: Figure 5 (a) shows the obtained gap structure in the case of $g = 0$ and $U = 0.439$ ($\alpha_s = 0.98$) in the $k_z = \pi$ -plane. The gap functions are almost independent of k_z , except that h-FS1,2 exist only for $k_z \sim \pi$. The obtained gap structure is essentially independent even if smaller U is used. Similarly to the previous study in Ref. [30], the gap functions on the h-FS1,2 are very small. However, this result is opposite to the experimental data

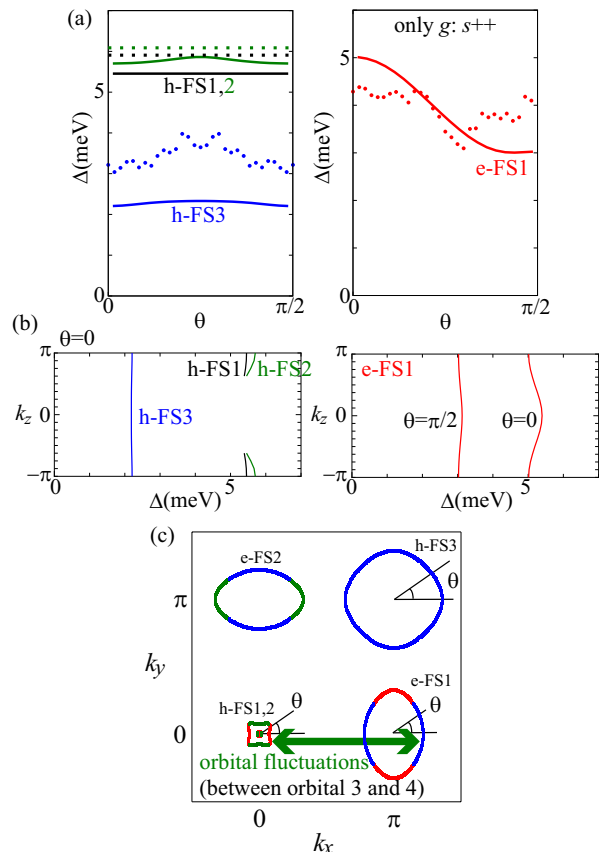


FIG. 4: (Color online) (a) Obtained s_{++} -wave gap functions for $U = 0$ and $g = 0.129$ in the $k_z = \pi$ -plane. The eigenvalue is $\lambda_E = 0.64$. The dotted lines represent the experimental data given by the ARPES measurement in Ref. [23]. (b) k_z -dependence of the gap functions. (c) Explanation for the orbital dependence of the gap functions due to orbital fluctuations.

shown by dotted lines. The k_z -dependence of the gap functions for $\theta = \pi/4$ are shown in Fig. 5 (b). All gaps depend on k_z only slightly.

In addition, the obtained θ -dependence of the gap on the e-FS1 is very different from the experimental data. Both Δ_3^h and Δ_1^e show the maximum values at $\theta \approx \pi/4$, because of the reason that they are connected by the wavevector of the spin fluctuations $\mathbf{Q} \approx (\pi, 0), (0, \pi)$ shown in Fig. 5 (c). In addition, the gap function of h-FS3 has eight nodes inconsistently with experiments. We verified these eight nodes disappear by using larger value of $J/U \sim 0.4$ ($U' = U - 2J \sim 0.2U$) as used in Ref. [30].

In Appendix A, we show the s_{\pm} -wave gap for smaller U ($\alpha_s = 0.90$). In this case, the magnitude of $\Delta_{1,2}^h$ becomes relatively large. On the other hand, the nodal gap appears on the e-FSs, inconsistently with experiments. Thus, the overall experimental data is difficult to be explained by the spin fluctuation theory.

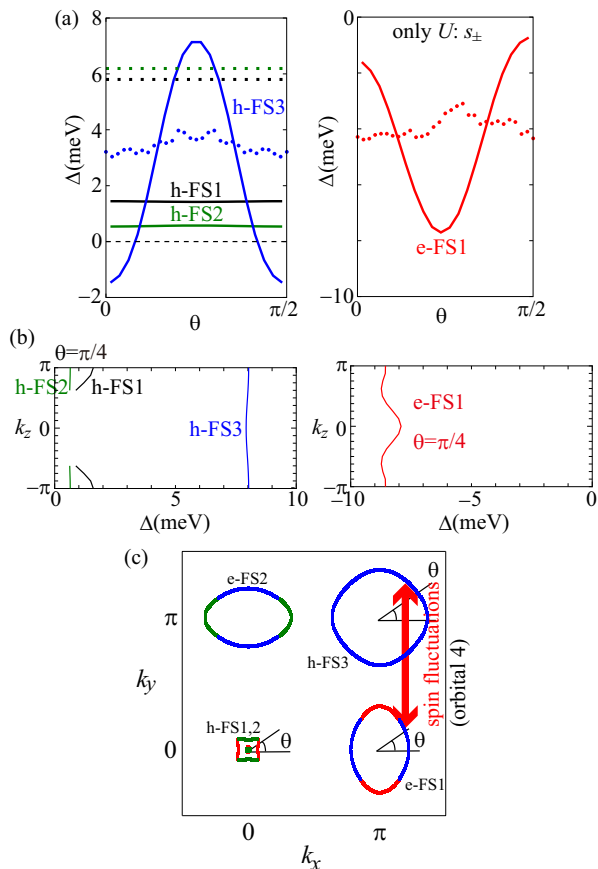


FIG. 5: (Color online) (a) Obtained s_{\pm} -wave gap functions for $U = 0.439$ and $g = 0$ in the $k_z = \pi$ -plane. The eigenvalue is $\lambda_E = 0.79$. (b) k_z -dependence of the gap functions. (c) Explanation for the orbital dependence of the gap functions due to spin fluctuations.

C. Coexistence of orbital and spin fluctuations: s_{++} -wave and hole- s_{\pm} -wave states

Now, we discuss the superconducting state when the orbital and spin fluctuations coexist. In the case of $\text{BaFe}_2(\text{As,P})_2$, the coexistence of both fluctuations produces the three-dimensional loop-shape nodes on electron-like FSs, as discussed in Ref. [35]. In the present model for LiFeAs , we find that the coexistence of orbital and spin fluctuations leads to a very exotic s -wave state, since the band structure of LiFeAs is very different from that of $\text{BaFe}_2(\text{As,P})_2$.

Figure 6 (a) shows the obtained gap functions in the case of $g = 0.125$ and $U = 0.200$. The obtained Stoner factors are $\alpha_c = 0.98$ and $\alpha_s = 0.45$. In this case, the orbital fluctuations are much larger than the spin fluctuations, and therefore we obtain the s_{++} -wave state. Except for h-FS3, the obtained gap structures are similar to those of the “pure s_{++} -wave state” without U in Fig. 4. Due to the moderate spin fluctuations on the d_{xy} -orbital, the anisotropy of Δ_3^h is enlarged, consistently with experimental results.

If we increase the value of U further, we obtain a highly nontrivial gap structure with sign-reversal within the h-FSS: Figure 6 (b) shows the obtained gap functions in the case of $g = 0.122$ and $U = 0.380$ ($\alpha_c = 0.98$ and $\alpha_s = 0.85$). Here, only Δ_3^h is negative. In this “hole- s_{\pm} -wave state” with “sign-reversal within hole-pockets”, the obtained gap structures of $\Delta_{1,2}^h$ and $\Delta_{1,2}^e$ are qualitatively similar to those in the s_{++} -wave state in Fig. 4. On the other hand, Δ_3^h becomes very anisotropic, similarly to Δ_3^h in the s_{\pm} -wave state in Fig. 5.

We discuss the reason why hole- s_{\pm} -wave is realized by the coexistence of orbital and spin fluctuations: In the present hole- s_{\pm} -wave state, as shown in Fig. 6 (c), $\Delta_{1,2}^h \cdot \Delta_{1,2}^e$ is positive due to orbital fluctuations, whereas $\Delta_3^h \cdot \Delta_{1,2}^e$ is negative due to spin fluctuations. The obtained gap structure is qualitatively consistent with ARPES measurement in Ref. [23], although the gap structures of the s_{++} -wave state in Fig. 4 are more consistent with experiments. The present mechanism of the “sign-reversal within hole-pockets” due to orbital+spin fluctuations would be realized in other Fe-based superconductors. In fact, the hole- s_{\pm} -wave state was first discussed in $\text{Ba}_{1-x}\text{K}_x\text{Fe}_2\text{As}_2$ based on the thermal conductivity and penetration depth measurements [32], in addition to the recent ARPES study [33].

Finally, we discuss on other theoretical works which predict the sign-reversal within hole-pockets. The hole- s_{\pm} -wave state was first discussed by the authors in Ref. [41], assuming the repulsive interaction between h-FSS and e-FSS in addition to the repulsive pairing interaction within the h-FSSs. For LiFeAs , similar scenario was discussed in Ref. [42], by introducing competing repulsive interactions, although the repulsive interaction within the h-FSSs is much weaker within the RPA because of the ill-nesting. Also, the authors in Ref. [43] discussed the orbital antiphase s^{+-} state, in which the sign-reversal within hole-pocket is realized due to the strong repulsion between d_{xy} and $d_{xz,yz}$ orbitals. In this state, the gap on e-FS is nodal in the unfolding picture, whereas it is fully-gapped in the present hole- s_{\pm} state in Fig. 6 (b).

References [41–43] considered the competition between two kinds of repulsive interactions. In contrast, in the present paper, the hole- s_{\pm} -wave state is explained in terms of the cooperation between the “attractive interaction among (d_{xz}, d_{yz})- and d_{xy} -orbitals” and “repulsive interaction on the d_{xy} -orbital”.

IV. SELF-CONSISTENT VC+ Σ (SC-VC $_{\Sigma}$) METHOD FOR THE HUBBARD MODEL ($g = 0$)

In previous sections, we studied the extended Hubbard model with multi-orbital Coulomb interaction ($U, U', J = (U - U')/2$) and quadrupole interaction (g). Here, orbital (spin) fluctuations are induced by g (U) and inter-orbital (intra-orbital) nesting of the FSs. Orbital fluctuations are the driving force of the fully-gapped s_{++} -wave state, and the coexistence of orbital and spin fluctuations gives

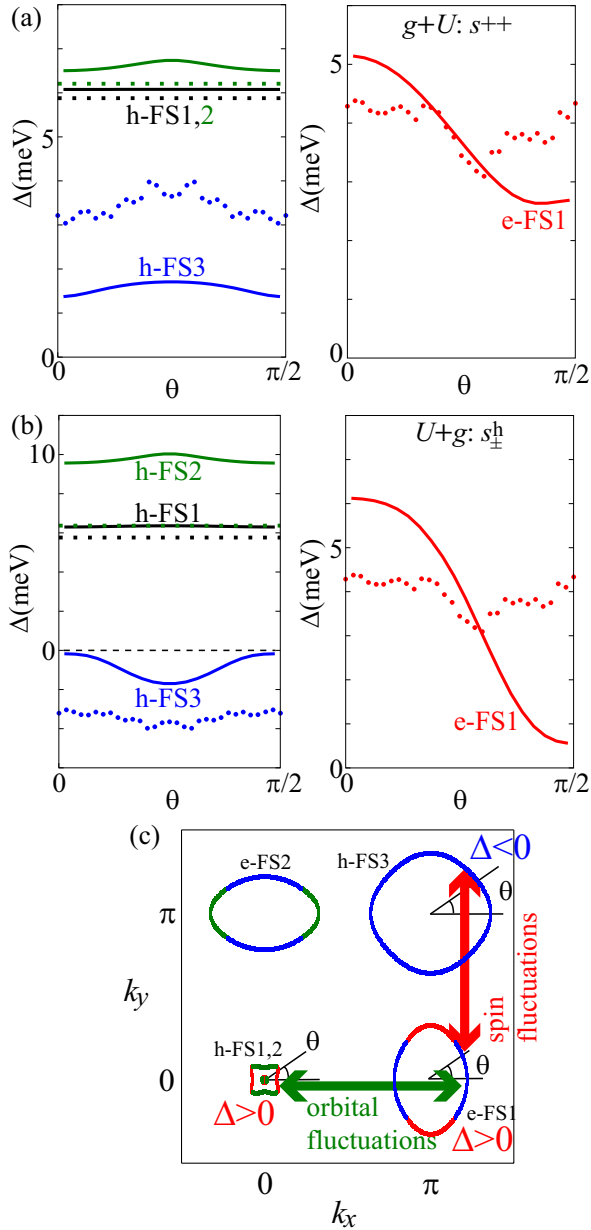


FIG. 6: (Color online) Obtained gap functions in the case of $U \neq 0$ and $g \neq 0$: (a) The s_{++} -wave state for $U = 0.200$ and $g = 0.125$ in the $k_z = \pi$ -plane. The eigenvalue is $\lambda_E = 0.47$. (b) The hole- s_{\pm} -wave state for $U = 0.380$ and $g = 0.122$ in the $k_z = \pi$ -plane, in which only the gap function on the h-FS3 is negative. The eigenvalue is $\lambda_E = 0.20$. (c) Origin of the hole- s_{\pm} -wave state due to the coexistence of the “orbital-fluctuations among (d_{xz}, d_{yz}) - and d_{xy} -orbitals” and the “spin-fluctuations on the d_{xy} -orbital”.

rise to the hole- s_{\pm} state with the sign-reversal within the hole-pockets.

In Ref. [15], we had shown that g is induced by in-plane Fe-ion oscillations. Consistently, kink structure in the quasiparticle dispersion due to Fe-ion oscillations is observed experimentally in LiFeAs [23]. Later, we

found that g is also induced by the Coulomb interaction (without e -ph interaction) beyond the RPA: It was revealed that the Aslamazov-Larkin type vertex correction (AL-VC) produce large effective quadrupole interaction g [16]. By solving the model for LiFeAsO using the self-consistent vertex correction (SC-VC) method, we obtain strong developments of $\chi_{x^2-y^2}^Q(\mathbf{q})$ at $q = (0, 0)$ and $\chi_{xz, yz}^Q(\mathbf{q})$ at $q = (0, \pi), (\pi, 0)$ [16]. The former fluctuations explain the orthorhombic structure transition in mother compounds [44].

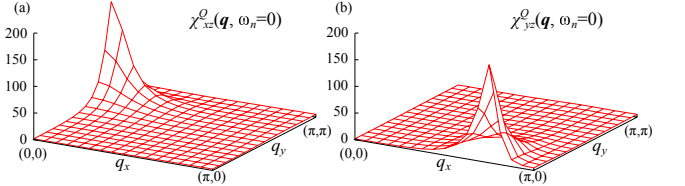


FIG. 7: (Color online) The quadrupole susceptibility $\chi_{xz}^Q(\mathbf{q})$ and $\chi_{yz}^Q(\mathbf{q})$ obtained by the SC-VC $_{\Sigma}$ method based on the Hubbard model. Other quadrupole fluctuations are small. The used parameters are $U = 0.96$, $J/U = 0.13$, and $g = 0$. The Stoner factors are $\alpha_c = 0.97$ and $\alpha_s = 0.87$.

In this section, we analyze the tight-binding Hubbard model ($g = 0$) for LiFeAs using the self-consistent VC+ Σ (SC-VC $_{\Sigma}$) method, which was used in Refs. [45, 46]. To simply the numerical calculation, we study the $k_z = \pi$ -plane of the present three-dimensional LiFeAs model. In the SC-VC $_{\Sigma}$ method, the self-energy matrix $\hat{\Sigma}$ is given by the one-loop approximation:

$$\Sigma_{lm}(k) = T \sum_q \sum_{l', m'} V_{ll', mm'}^{\Sigma}(q) G_{l'm'}(k-q), \quad (16)$$

where G is the full Green function with self-energy given as $\{\hat{G}(k)\}^{-1} = \{\hat{G}^{(0)}(k)\}^{-1} - \hat{\Sigma}(k)$. $\hat{V}^{\Sigma}(q)$ is the effective interaction for the self-energy: $\hat{V}^{\Sigma}(q) = \frac{3}{2}\hat{\Gamma}^s \hat{\chi}^s(q) \hat{\Gamma}^s + \frac{1}{2}\hat{\Gamma}^c \hat{\chi}^c(q) \hat{\Gamma}^c - \frac{1}{4}(\hat{\Gamma}^c - \hat{\Gamma}^s) \hat{\chi}^0(q) (\hat{\Gamma}^c - \hat{\Gamma}^s) - \frac{1}{8}(\hat{\Gamma}^c + \hat{\Gamma}^s) \hat{\chi}^0(q) (\hat{\Gamma}^c + \hat{\Gamma}^s)$. The third and fourth terms of the right hand side in $\hat{V}^{\Sigma}(q)$ are required to cancel the double counting in the 2nd order diagrams.

The susceptibility for the charge (spin) sector is

$$\hat{\chi}^{c(s)}(q) = \frac{\hat{\Phi}^{c(s)}(q)}{\hat{1} - \hat{\Gamma}^{c(s)} \hat{\Phi}^{c(s)}(q)}, \quad (17)$$

where $\hat{\Phi}^{c(s)}(q) \equiv \hat{\chi}_{\Sigma}^{(0)}(q) + \hat{X}^{c(s)}(q)$ is the irreducible susceptibility. $\hat{\chi}_{\Sigma}^{(0)}(q)$ is given by eq. (3), by replacing $\hat{G}^{(0)}$ with the full Green function \hat{G} . $\hat{X}^{c(s)}(q)$ is the VC for the charge (spin) sector. In the SC-VC $_{\Sigma}$ method, we calculate the VC up to the second-order terms with respect to the susceptibility $\chi^{s,c}$. The second-order term (=Aslamazov-Larkin term) is always dominant over the first-order term (=Maki-Thompson term), and the AL-VC for the charge sector is given as [16]

$$X_{ll', mm'}^c(q)$$

$$= \frac{T}{2} \sum_k \sum_{a \sim h} \Lambda_{ll',ab,ef}(q; k) \{V_{ab,cd}^c(k+q)V_{ef,gh}^c(-k) + 3V_{ab,cd}^s(k+q)V_{ef,gh}^s(-k)\} \Lambda'_{mm',cd,gh}(q; k), \quad (18)$$

where $\hat{V}^{s,c}(q) \equiv \hat{\Gamma}^{s,c} + \hat{\Gamma}^{s,c} \hat{\chi}^{s,c}(q) \hat{\Gamma}^{s,c}$, $\hat{\Lambda}(q; k)$ and $\hat{\Lambda}'(q; k)$ are the three-point vertex made of three Green functions given in Ref. [16]. We include all U^2 -terms without the double counting to obtain reliable results. Here, we neglect $\hat{X}^{AL,s}$ because the contribution of $\hat{X}^{AL,s}$ is much smaller than that of $\hat{X}^{AL,c}$ [16, 47, 48]. Also, we use $\hat{G}^{(0)}$ in calculating $\hat{\Lambda}$ and $\hat{\Lambda}'$ since they are underestimated at high temperatures ($T \gg 0.01$) due to large quasiparticle damping $\text{Im}\Sigma(\mathbf{q}, -i\delta) \propto T$.

In the SC-VC $_{\Sigma}$ method, we solve eqs. (16)-(18) self-consistently. Here, we study the two-dimensional model given by the $k_z = \pi$ plane of LiFeAs using the SC-VC $_{\Sigma}$ method. Figure 7 shows the obtained quadrupole susceptibility $\chi_{xz}^Q(\mathbf{q})$ and $\chi_{yz}^Q(\mathbf{q})$. The used parameters are $U = 0.96$, $J/U = 0.13$, $g = 0$, and $T = 0.02$. The obtained $\chi_{xz,yz}^Q(\mathbf{q})$ shows incommensurate peak structure, reflecting the bad nesting of the FSs in LiFeAs [49]. In highly contrast to the case of LaFeAsO [16], $\chi_{x^2-y^2}^Q(\mathbf{0})$ in the present model is very small, consistently with the absence of structure transition in LiFeAs. (We verified that very similar result is obtained by the SC-VC method (without self-energy correction) by putting $J/U \lesssim 0.09$.) Thus, the quadrupole interaction in eq. (2) is derived from the VC due to Coulomb interaction in addition to the e-ph interaction.

Theoretically, the $O_{xz/yz}$ type quadrupole fluctuations are easily realized because of the good inter-orbital nesting of the FSs. They are produced by taking account of the small quadrupole interaction g and/or the AL term due to Coulomb interaction. In fact, both AL term and g contribute to the $O_{xz/yz}$ -type quadrupole fluctuations cooperatively [16], indicating that the phenomenological interaction g can be used as a substitute for the AL term.

In Ref. [46], we solved the gap equation based on the “two-dimensional” model for LaFeAsO $_{1-x}$ H $_x$ using the SC-VC $_{\Sigma}$ method, and obtained various types of s -wave superconducting states, like s_{++} , s_{\pm} , and hole- s_{\pm} -wave states, due to the cooperation of orbital and spin fluctuations. It is our future problem to study the “three-dimensional” gap structure of LiFeAs based on the SC-VC $_{\Sigma}$ method. In LiFeAs, it is naively expected that strong incommensurate orbital fluctuations shown in Fig. 7 produces large $\Delta_{1,2}^h$ like in Fig. 4 (a), since h-FS1,2 (made of $d_{xz,yz}$ -orbitals) and e-FS1,2 (made of d_{xy} -orbital) are connected by these incommensurate orbital fluctuations.

V. SUMMARY

In this paper, we studied the three-dimensional five-orbital model of LiFeAs based on the recently-developed orbital-spin fluctuation theories [15, 16]. It is found that

the experimentally observed gap structure of LiFeAs in Ref. [23] is quantitatively reproduced in terms of the orbital-fluctuation mechanism. Especially, the largest gap on h-FS1 and h-FS2 in Fig. 1 (b) is naturally reproduced by the inter-orbital fluctuations, as demonstrated in Figs. 4 (a) and 9, whereas it is unable to be explained by the spin fluctuation scenario. Therefore, the largest gap on h-FS1,2 is the hallmark of the orbital-fluctuation-mediated superconductivity in LiFeAs. Also, the orbital-independent isotropic gap (absence of horizontal node) on h-FSs in Ba122 [36, 37] and Sr122 indicates the important role of orbital fluctuations on the pairing mechanism [35].

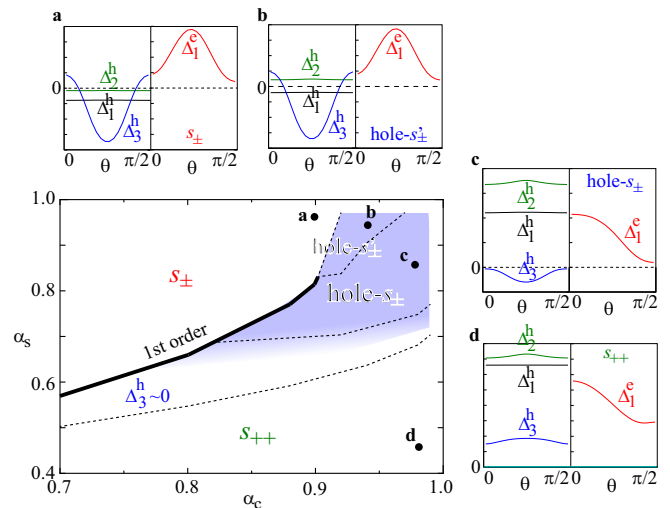


FIG. 8: (Color online) α_c - α_s phase diagram of the gap structure in LiFeAs. The gap structure at each point **a**-**d** is shown in the figure. Each s_{\pm} -wave, s_{++} -wave, and hole- s_{\pm} -wave state is realized in wide parameter region. In the region “ $\Delta_3^h \sim 0$ ”, the gaps on other FSs have the same sign, so nearly s_{++} -wave state is realized. In the “hole- s'_{\pm} -wave gap” state at point **b**, $\Delta_1^h \cdot \Delta_2^h$ is negative, and both $|\Delta_1^h|$ and $|\Delta_2^h|$ are very small.

When orbital and spin fluctuations coexist, the “hole- s_{\pm} -wave state” is obtained, in which only the gap of the largest d_{xy} -orbital hole-pocket is sign-reversed. We expect that the present mechanism of the “sign-reversal within hole-pockets” due to orbital+spin fluctuations would be realized in other Fe-based superconductors, although LiFeAs might not be the case. In fact, the realization of the hole- s_{\pm} -wave state was first discussed in Ba $_{1-x}$ K $_x$ Fe $_2$ As $_2$ based on the thermal conductivity and penetration depth measurements [32]. The hole- s_{\pm} -wave is naturally realized under the coexistence of the “spin-fluctuations on the d_{xy} -orbital” and the “orbital-fluctuations among the (d_{xz} , d_{yz})- and d_{xy} -orbitals”.

Figure 8 shows the obtained α_c - α_s phase diagram of the gap structure in LiFeAs. As expected, the s_{\pm} -wave state (s_{++} -wave state) is realized for wide region of $\alpha_s > \alpha_c$ ($\alpha_c > \alpha_s$). When both α_s and α_c are close to unity, we obtain the hole- s_{\pm} -wave gap in a wide region. The

gap structure at each point $\mathbf{a}\sim\mathbf{d}$ is shown in the figure. In the region “ $\Delta_3^h \sim 0$ ”, obtained $\Delta_3^h(\theta)$ is nodal and very small in magnitude, and it is close to the s_{++} -wave state in that other gaps are positive and large. In the “hole- s'_{\pm} -state” at point \mathbf{b} , Δ_1^h and Δ_2^h are opposite in sign, and both $|\Delta_1^h|$ and $|\Delta_2^h|$ are very small. Therefore, various types of s -wave gap structure are realized due to the cooperation of orbital and spin fluctuations.

We also applied the SC-VC $_{\Sigma}$ method to the Hubbard model of LiFeAs, and obtained the strong development of antiferro-orbital fluctuations due to the AL-type VC. In contrast, the ferro-orbital fluctuations remain small contrary to the previous study for La1111 [16], consistently with the absence of orthorhombic structure transition in LiFeAs. It is our important future issue to study the superconducting state of LiFeAs based on the SC-VC $_{\Sigma}$ method.

Acknowledgments

This study has been supported by Grants-in-Aid for Scientific Research from MEXT of Japan. S.V.B. and V.B.Z. acknowledge support under Grants No. ZA 654/1-1, No. BO1912/2-2, and No. BE1749/13. Part of numerical calculations were performed on the Yukawa Institute Computer Facility.

Appendix A: Gap Structure due to Moderate Orbital and Spin Fluctuations

In Sec. III, we have shown the gap structures of the s_{++} -wave and s_{\pm} -wave states in the presence of very large orbital and spin fluctuations; $\alpha_{c,s} = 0.98$. However, we have very little experimental information on the strength of fluctuations in LiFeAs. In fact, the spin fluctuations are moderate according to NMR measurement [26] and neutron scattering measurement [27–29]. In this Appendix, we analyze the gap equation for smaller orbital and spin fluctuations, and show that the obtained gap structures in Sec. III are essentially unchanged even when the fluctuations are moderate.

Figure 9 shows the s_{++} -wave gap functions for $g = 0.118$ and $U = 0$. In this case, $\alpha_c = 0.90$ and $\max_{\mathbf{q}} \chi_{xz}^Q(\mathbf{q}, 0) \approx 38$. The obtained gap structure is very similar to that in Fig. 4 (a) for $\alpha_c = 0.98$. Especially, experimentally observed local maximum at $\theta = \pi/2$ on the e-FS3 is well reproduced in Fig. 9. Thus, the s_{++} -wave gap structure is essentially unchanged for $\alpha_c \geq 0.90$, although the eigenvalue λ_E increases as α_c approaches unity. The obtained eigenvalue $\lambda_E = 0.34$ is relatively large, which means that moderate orbital fluctuations ($\alpha_c = 0.90$) would be enough to induce the superconductivity.

Figure 10 shows the s_{\pm} -wave gap functions for $U = 0.403$ and $g = 0$. In this case, $\alpha_s = 0.90$ and $\max_{\mathbf{q}} \chi^s(\mathbf{q}, 0) \approx 35$. As for the hole-pockets, the obtained

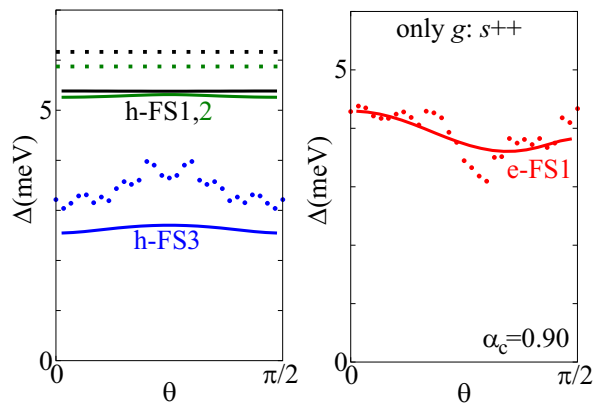


FIG. 9: (Color online) Obtained s_{++} -wave gap structure for $U = 0$ and $g = 0.118$ ($\alpha_c = 0.90$) in the $k_z = \pi$ -plane. The eigenvalue is $\lambda_E = 0.34$. The dotted lines represent the experimental data given by the ARPES measurement in Ref. [23].

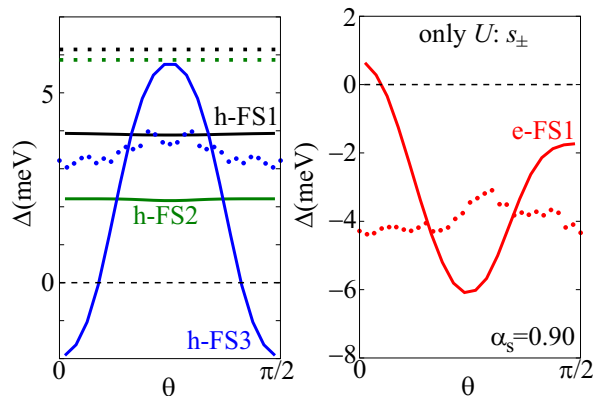


FIG. 10: (Color online) Obtained s_{\pm} -wave gap structure for $U = 0.403$ and $g = 0$ ($\alpha_s = 0.90$) in the $k_z = \pi$ -plane. The eigenvalue is $\lambda_E = 0.12$.

gap functions are essentially similar to those in Fig. 5 for $\alpha_s = 0.98$, except that $\Delta_{1,2}^h$ becomes relatively large. As for the electron-pocket, the nodal gap appears on the e-FSS, although it is inconsistent with experiments. Thus, the overall experimental data is difficult to be explained by the spin fluctuation theory for $\alpha_s \geq 0.90$.

Appendix B: Five-Orbital Tight-Binding Model for LiFeAs

Here, we explain the five-orbital tight-binding model for LiFeAs, which is given in unfolding the ten-orbital model given in Ref. [30]. The ten-orbital model in Ref. [30] is obtained by fitting the experimental band structure of LiFeAs in Ref. [23] near the Fermi level. The five-orbital model (single Fe unit cell) is obtained by unfolding the ten-orbital model (two-Fe unit cell), according to the procedure in Ref. [25]. The FSs of both

$(l,m) \backslash \mathbf{R}$	[0,0,0]	[1,0,0]	[1,1,0]	[2,0,0]	[2,1,0]	[2,2,0]	[0,0,1]	[1,0,1]	[2,0,1]	$\sigma_y I$	σ_d	
(1,1)	-0.305									+	+	+
(1,2)			-0.101							-	-	+(1,3)
(1,3)		0.100	-0.101							+	-	+(1,2)
(1,4)			-0.090							-	+	+
(1,5)		-0.162								+	+	-
(2,2)	-0.008	-0.050	0.152	-0.004	-0.040	-0.005	-0.003	-0.012		+	+	+(3,3)
(2,3)			0.090							-	+	+
(2,4)		-0.155	-0.064							+	-	+(3,4)
(2,5)			-0.010							-	-	-(3,5)
(3,3)	-0.008	-0.210	0.152	-0.051	0.053	-0.005	-0.003		0.011	+	+	+(2,2)
(3,4)			-0.064							-	-	+(2,4)
(3,5)		0.193	0.010							+	-	-(2,5)
(4,4)	0.020	0.019	0.030	-0.010	-0.004		0.011	0.004		+	+	+
(4,5)										-	+	-
(5,5)	-0.261	0.223	0.070							+	+	+

TABLE I: Hopping integrals for $\mathbf{R} = (x, y, z)$ for the present five-orbital model for LiFeAs. Notations are the same as those introduced in Refs. [11, 25]. σ_y , I , and σ_d corresponds to $t(x, -y, z; l, m)$, $t(-x, -y, z; l, m)$, and $t(y, x, z; l, m)$, respectively. Here, ‘ \pm ’ and ‘ $\pm(l', m')$ ’ in the row of (l, m) mean that the corresponding hopping is equal to $\pm t(x, y, z; l, m)$ and $\pm t(x, y, z; l', m')$, respectively. Notice also $t(\mathbf{R}; l, m) = t(-\mathbf{R}; m, l)$.

models are shown in Fig. 1 (a) and (b), respectively. Both models are equivalent, and the former model is more convenient for the numerical study. The FSs and band structure are given in Fig. 1. This experimental FSs of LiFeAs are very different from the FSs given by the density functional theory (DFT), in which FS1,2 predicted by the DFT are much larger. Better agreement between theory and ARPES is achieved by the LDA+DMFT study [50], since the FS1,2 shrinks due to the orbital-dependent self-energy that is absent in the LDA. As for the de Haas-van Alphen (dHvA) measurements, Ref. [51] showed reasonable agreement with the

DFT for the e-FSSs, and Ref. [52] reported the presence of very small three-dimensional hole-pockets, which would corresponds to h-FS1,2 in Fig. 1. The hopping parameters of the present model, $t^{l,m}(\mathbf{R}_a)$ in eq. (1), are listed in Table I.

Based on the LDA bandstructure, $\Delta_{1,2}^h$ in the spin fluctuation mediated s_{\pm} -wave state can become as large as other gaps, as discussed in Refs. [30, 53]. However, $\Delta_{1,2}^h$ in the s_{\pm} -wave state becomes very small based on the “experimental bandstructure”, as shown in Ref. [30] and in the present paper.

-
- [1] N. Fujiwara, S. Tsutsumi, S. Imura, S. Matsuishi, H. Hosono, Y. Yamakawa, and H. Kontani, Phys. Rev. Lett. **111**, 097002 (2013).
- [2] Y. Nakai, T. Iye, S. Kitagawa, K. Ishida, H. Ikeda, S. Kasahara, H. Shishido, T. Shibauchi, Y. Matsuda, and T. Terashima, Phys. Rev. Lett. **105**, 107003 (2010).
- [3] R. Zhou, Z. Li, J. Yang, D. L. Sun, C. T. Lin, and G. Zheng, Nat. Commun **4**, 3265, (2013).
- [4] R.M. Fernandes, L. H. VanBebber, S. Bhattacharya, P. Chandra, V. Keppens, D. Mandrus, M.A. McGuire, B.C. Sales, A.S. Sefat and J. Schmalian, Phys. Rev. Lett. **105**, 157003 (2010).
- [5] M. Yoshizawa, R. Kamiya, R. Onodera, Y. Nakanishi, K. Kihou, H. Eisaki and C. H. Lee, Phys. Soc. Jpn. **81**, 024604 (2012).
- [6] A. E. Böhrer, P. Burger, F. Hardy, T. Wolf, P. Schweiss, R. Fromknecht, M. Reinecker, W. Schranz, and C. Meingast, Phys. Rev. Lett. **112**, 047001 (2014).
- [7] Y. Gallais, R. M. Fernandes, I. Paul, L. Chauviere, Y.-X. Yang, M.-A. Measson, M. Cazayous, A. Sacuto, D. Colson, and A. Forget, Phys. Rev. Lett. **111**, 267001 (2013).
- [8] Y. Mizuguchi and Y. Takano, J. Phys. Soc. Jpn. **79**, 102001 (2010).
- [9] A. A. Kordyuk, V. B. Zabolotnyy, D. V. Evtushinsky, A. N. Yaresko, B. Büchner, and S. V. Borisenko, J. Supercond. Nov. Magn. **26**, 2837 (2013).
- [10] J. Maletz, V. B. Zabolotnyy, D. V. Evtushinsky, S. Thirupathaiah, A. U. B. Wolter, L. Harnagea, A. N. Yaresko, A. N. Vasiliev, D. A. Chareev, E. D. L. Rienks, B. Büchner, and S. V. Borisenko, Phys. Rev. B **89**, 220506(R) (2014).
- [11] K. Kuroki, S. Onari, R. Arita, H. Usui, Y. Tanaka, H. Kontani, and H. Aoki, Phys. Rev. Lett. **101**, 087004 (2008).
- [12] I. I. Mazin, D.J. Singh, M.D. Johannes, and M.H. Du, Phys. Rev. Lett. **101** (2008) 057003.
- [13] P. J. Hirschfeld, M. M. Korshunov, and I. I. Mazin, Rep. Prog. Phys. **74**, 124508 (2011).

- [14] A. V. Chubukov, D. V. Efremov, and I. Eremin, Phys. Rev. B **78**, 134512 (2008).
- [15] H. Kontani and S. Onari, Phys. Rev. Lett. **104**, 157001 (2010).
- [16] S. Onari and H. Kontani, Phys. Rev. Lett. **109**, 137001 (2012).
- [17] M. Sato, Y. Kobayashi, S. C. Lee, H. Takahashi, E. Satomi, and Y. Miura, J. Phys. Soc. Jpn. **79** (2009) 014710; S. C. Lee, E. Satomi, Y. Kobayashi, and M. Sato, J. Phys. Soc. Jpn. **79** (2010) 023702.
- [18] J. Li, Y.F. Guo, S.B. Zhang, J. Yuan, Y. Tsujimoto, X. Wang, C.I. Sathish, Y. Sun, S. Yu, W. Yi, K. Yamaura, E. Takayama-Muromachi, Y. Shirako, M. Akaogi, and H. Kontani, Phys. Rev. B **85**, 214509 (2012).
- [19] Y. Nakajima, T. Taen, Y. Tsuchiya, T. Tamegai, H. Kitamura, and T. Murakami, Phys. Rev. B **82**, 220504 (2010).
- [20] S. Onari and H. Kontani, Phys. Rev. Lett. **103**, 177001 (2009).
- [21] Y. Yamakawa, S. Onari and H. Kontani, Phys. Rev. B **87**, 195121 (2013).
- [22] S. Onari, H. Kontani, and M. Sato, Phys. Rev. B **81**, 060504(R) (2010); S. Onari and H. Kontani, Phys. Rev. B **84**, 144518 (2011).
- [23] S.V. Borisenko, V.B. Zabolotnyy, A.A. Kordyuk, D.V. Evtushinsky, T.K. Kim, I.V. Morozov, R. Follath and B. Büchner, Symmetry **4**, 251 (2012).
- [24] K. Umezawa, Y. Li, H. Miao, K. Nakayama, Z.-H. Liu, P. Richard, T. Sato, J. B. He, D.-M. Wang, G. F. Chen, H. Ding, T. Takahashi, and S.-C. Wang, Phys. Rev. Lett. **108**, 037002 (2012).
- [25] T. Miyake, K. Nakamura, R. Arita and M. Imada, J. Phys. Soc. Jpn. **79**, 044705 (2010).
- [26] Li Zheng, Ooe Yosuke, Wang Xian-Cheng, Liu Qing-Qing, Jin Chang-Qing, Ichioka Masanori, Zheng Guo-qing, J. Phys. Soc. Jpn **79**, 083702 (2010).
- [27] N. Qureshi, P. Steffens, Y. Drees, A.C. Komarek, D. Lamago, Y. Sidis, L. Harnagea, H.-J. Grafe, S. Wurmehl, B. Büchner, and M. Braden, Phys. Rev. Lett. **108**, 117001 (2012).
- [28] J. Knolle, V. B. Zabolotnyy, I. Eremin, S. V. Borisenko, N. Qureshi, M. Braden, D. V. Evtushinsky, T. K. Kim, A. A. Kordyuk, S. Sykora, Ch. Hess, I. V. Morozov, S. Wurmehl, R. Moessner, and B. Büchner, Phys. Rev. B **86**, 174519 (2012).
- [29] A. Taylor, et al., Phys. Rev. B **83**, 220514 (2011).
- [30] Y. Wang, A. Kreisell, V. B. Zabolotnyy, S. V. Borisenko, B. Büchner, T. A. Maier, P. J. Hirschfeld, and D. J. Scalapino, Phys. Rev. B **88**, 174516 (2013).
- [31] M. P. Allan, A. W. Rost, A. P. Mackenzie, Yang Xie, J. C. Davis, K. Kihou, C. H. Lee, A. Iyo, H. Eisaki, and T.-M. Chuang, Science **336**, 563 (2012).
- [32] D. Watanabe, T. Yamashita, Y. Kawamoto, S. Kurata, Y. Mizukami, T. Ohta, S. Kasahara, M. Yamashita, T. Saito, H. Fukazawa, Y. Kohori, S. Ishida, K. Kihou, C. H. Lee, A. Iyo, H. Eisaki, A. B. Vorontsov, T. Shibauchi, and Y. Matsuda, Phys. Rev. B **89**, 115112 (2014).
- [33] P. Zhang, P. Richard, T. Qian, X. Shi, J. Ma, L.-K. Zeng, X.-P. Wang, E. Rienks, C.-L. Zhang, Pengcheng Dai, Y.-Z. You, Z.-Y. Weng, X.-X. Wu, J. P. Hu, and H. Ding, arXiv:1312.7064.
- [34] K. Suzuki, H. Usui, and K. Kuroki, J. Phys. Soc. Jpn. **80**, 013710 (2011).
- [35] T. Saito, S. Onari, and H. Kontani, Phys. Rev. B **88**, 045115 (2013).
- [36] T. Shimojima, F. Sakaguchi, K. Ishizaka, Y. Ishida, T. Kiss, M. Okawa, T. Togashi, C.-T. Chen, S. Watanabe, M. Arita, K. Shimada, H. Namatame, M. Taniguchi, K. Ohgushi, S. Kasahara, T. Terashima, T. Shibauchi, Y. Matsuda, A. Chainani, and S. Shin, Science **332**, 564 (2011).
- [37] T. Yoshida, S. Ideta, T. Shimojima, W. Malaeb, K. Shinada, H. Suzuki, I. Nishi, A. Fujimori, K. Ishizaka, S. Shin, Y. Nakashima, H. Anzai, M. Arita, A. Ino, H. Namatame, M. Taniguchi, H. Kumigashira, K. Ono, S. Kasahara, T. Shibauchi, T. Terashima, Y. Matsuda, M. Nakajima, S. Uchida, Y. Tomioka, T. Ito, K. Kihou, C. H. Lee, A. Iyo, H. Eisaki, H. Ikeda, R. Arita, T. Saito, S. Onari, and H. Kontani, arXiv:1301.4818.
- [38] M. Yamashita, Y. Senshu, T. Shibauchi, S. Kasahara, K. Hashimoto, D. Watanabe, H. Ikeda, T. Terashima, I. Vekhter, A. B. Vorontsov, and Y. Matsuda, Phys. Rev. B **84**, 060507(R) (2011).
- [39] T. Takimoto, T. Hotta, T. Maehira and K. Ueda, J. Phys. Condens. Matter **14**, L369 (2002).
- [40] S. Graser, A. F. Kemper, T. A. Maier, H.-P. Cheng, P. J. Hirschfeld, and D. J. Scalapino, New Journal of Physics. **12**, 073030 (2010).
- [41] S. Maiti and A. V. Chubukov, Phys. Rev. B **87**, 144511 (2013).
- [42] F. Ahn, I. Eremin, J. Knolle, V.B. Zabolotnyy, S.V. Borisenko, B. Büchner, A.V. Chubukov, arXiv:1402.2112.
- [43] Z. P. Yin, K. Haule, G. Kotliar, arXiv:1311.1188.
- [44] H. Kontani and Y. Yamakawa, arXiv:1312.0528
- [45] S. Onari, H. Kontani, S. V. Borisenko, V.B. Zabolotnyy and B. Büchner, arXiv:1307.6119.
- [46] S. Onari, Y. Yamakawa and H. Kontani, arXiv:1312.0481 (Phys. Rev. Lett. (2014)).
- [47] Y. Ohno, M. Tsuchiizu, S. Onari, and H. Kontani, J. Phys. Soc. Jpn. **82**, 013707 (2013).
- [48] M. Tsuchiizu, Y. Ohno, S. Onari, and H. Kontani, Phys. Rev. Lett. **111**, 057003 (2013).
- [49] In Ref. [45], the quadrupole susceptibility $\chi_{yz}(\mathbf{q}) \propto \chi_{2,4;4,2}(\mathbf{q})$ given by the SC-VC $_{\Sigma}$ method has commensurate peak at $\mathbf{q} = (\pi, 0)$, since the calculation temperature is rather high.
- [50] Z. Yin, K. Haule, and G. Kotliar, Nat. Mater. **10**, 932 (2011); J. Ferber, K. Foyevtsova, R. Valenti, and H. O. Jeschke, Phys. Rev. B **85**, 094505 (2012); G. Lee *et al.*, Phys. Rev. Lett. **109**, 177001 (2012).
- [51] C. Putzke, et al., Phys. Rev. Lett. **108**, 047002 (2012).
- [52] B. Zeng, et al., Phys. Rev. B **88**, 144518 (2013).
- [53] C. Platt, R. Thomale, and W. Hanke, Phys. Rev. B **84**, 235121 (2011).